Published in final edited form as:
Biochim Biophys Acta Mol Cell Res. 2019 March ; 1866(3): 337–348. doi:10.1016/j.bbamcr.2018.08.017.

N-acetylaspartate pathway is nutrient responsive and coordinates lipid and energy metabolism in brown adipocytes

Katharina Huber[a,b,c], **Dina C. Hofer**[a], **Sophie Trefely**[b,c,d], **Helmut J. Pelzmann**[a,1], **Corina Madreiter-Sokolowski**[e], **Madalina Duta-Mare**[e], **Stefanie Schlager**[e,2], **Gert Trausinger**[f], **Sarah Stryeck**[e], **Wolfgang F. Graier**[e,h], **Dagmar Kolb**[g], **Christoph Magnes**[f], **Nathaniel W. Snyder**[d], **Andreas Prokesch**[g,h], **Dagmar Kratky**[e,h], **Tobias Madl**[e,h], **Kathryn E. Wellen**[b,c], and **Juliane G. Bogner-Strauss**[a,h,*]

[a]Institute of Biochemistry, Graz University of Technology, Graz, Austria

[b]Department of Cancer Biology, University of Pennsylvania, Philadelphia, USA

[c]Abramson Family Cancer Research Institute, University of Pennsylvania, Philadelphia, USA

[d]AJ Drexel Autism Institute, Drexel University, Philadelphia, USA

[e]Gottfried Schatz Research Center for Cell Signaling, Metabolism and Aging, Cell Biology, Molecular Biology and Biochemistry, Medical University of Graz, Graz, Austria

[f]HEALTH Institute for Biomedicine and Health Sciences, Joanneum Research, Graz, Austria

[g]Gottfried Schatz Research Center for Cell Signaling, Metabolism and Aging, Cell Biology, Histology and Embryology, Medical University of Graz, Graz, Austria

[h]BioTechMed-Graz, Graz, Austria

Abstract

The discovery of significant amounts of metabolically active brown adipose tissue (BAT) in adult humans renders it a promising target for anti-obesity therapies by inducing weight loss through increased energy expenditure. The components of the *N*-acetylaspartate (NAA) pathway are highly abundant in BAT. Aspartate *N*-acetyltransferase (Asp-NAT, encoded by *Nat8l*) synthesizes NAA from acetyl-CoA and aspartate and increases energy expenditure in brown adipocytes. However, the exact mechanism how the NAA pathway contributes to accelerated mobilization and oxidation of lipids and the physiological regulation of the NAA pathway remained elusive. Here, we

*Corresponding author at: Graz University of Technology, Institute of Biochemistry, Humboldtstrasse 46/3, 8010 Graz, Austria. juliane.bogner-strauss@tugraz.at (J.G. Bogner-Strauss).
[1]Present address: Fresenius Kabi Austria GmbH, Graz, Austria.
[2]Present address: Boehringer Ingelheim RCV GmbH & Co KG, Vienna, Austria.

Author contributions

The project was conceptualized and designed by K.H. and J.G.B.-S. K.H., D.C.H., S.T., H.J.P., C.T.M.-S, M.D.-M., S.Sc., G.T., S.St. performed the experiments and analyzed data with support of W.F.G., D.Ko., C.M., N.W.S., A.P., D.Kr., T.M., K.E.W. and J.G.B.-S. K.H and J.G.B.-S. wrote the manuscript. All authors read and provided feedback on manuscript and figures.

Conflict of interest

The authors declare no potential conflict of interest.

Transparency document

The Transparency document associated with this article can be found, in online version.

Europe PMC Funders Author Manuscripts

demonstrate that the expression of NAA pathway genes corresponds to nutrient availability and specifically responds to changes in exogenous glucose. NAA is preferentially produced from glucose-derived acetyl-CoA and aspartate and its concentration increases during adipogenesis. Overexpression of *Nat8l* drains glucose-derived acetyl-CoA into the NAA pool at the expense of cellular lipids and certain amino acids. Mechanistically, we elucidated that a combined activation of neutral and lysosomal (acid) lipolysis is responsible for the increased lipid degradation. Specifically, translocation of the transcription factor EB to the nucleus activates the biosynthesis of autophagosomes and lysosomes. Lipid degradation within lysosomes accompanied by adipose triglyceride lipase-mediated lipolysis delivers fatty acids for the support of elevated mitochondrial respiration. Together, our data suggest a crucial role of the NAA pathway in energy metabolism and metabolic adaptation in BAT.

Keywords

N-acetyltransferase 8-like; Asp-NAT; Aspartoacylase; *N*-acetylaspartate; Brown adipocytes; Lipophagy; Energy expenditure; Fatty acid metabolism; Lipid metabolism

1 Introduction

The worldwide epidemic of obesity is primarily caused by increased food intake, sedentary lifestyle, and genetic predisposition. These conditions cause an imbalance between energy consumption and energy expenditure resulting in a massive accumulation of fat, predominantly in white adipose tissue (WAT) [1]. Conversely, brown adipose tissue (BAT) is specialized to increase energy expenditure and is a promising target for interventions to combat obesity [2]. BAT has the ability to oxidize high amounts of glucose and fatty acids (FA) [3]. The mobilization of FA from cellular lipid stores requires the enzymatic hydrolysis of triacylglycerols (TG) by neutral or acid lipolysis, which are classified depending on the pH-optimum of the involved enzymes [4,5]. Neutral lipid hydrolysis is mediated by a lipolytic cascade consisting of adipose triglyceride lipase (ATGL) [6–8], hormone-sensitive lipase (HSL) and monoacylglycerol lipase (MGL) [9]. ATGL specifically catabolizes TG generating free FA and diacylglycerol (DG). Hormone-sensitive lipase (HSL) is capable of hydrolyzing a broad substrate spectrum with highest activities toward DG and cholesterol ester. The last step of neutral lipolysis is facilitated by monoacylglycerol lipase, which converts monoacylglycerols to FAs and glycerol [4,9]. In BAT, lipophagy substantially contributes to TG degradation [10,11]. Lipophagy is a specialized form of macroautophagy and defined as the autophagic degradation of intracellular lipid droplets in the lysosome [12]. To this end, cytosolic cargo is engulfed by double membrane vesicles (autophagosomes) that ultimately fuse with lysosomes for degradation of *e.g.* TG carried out by lysosomal acid lipase (LAL) [13,14].

The important role of BAT in maintaining body temperature through the uncoupling protein 1 (UCP1)-mediated thermogenesis in rodents and infants has long been recognized [15]. The more recent discovery of significant amounts of metabolically active BAT in adult humans has revealed additional roles for BAT in the maintenance of energy homeostasis [16,17]. However, the metabolic pathways that respond to and regulate energy homeostasis in BAT

are not well defined. Thus, it is of critical importance to understand novel metabolic pathways that control energy homeostasis in BAT to counteract obesity [18].

We previously identified the *N*-acetylaspartate (NAA) pathway as highly abundant in BAT [19]. Previously, the NAA pathway was extensively investigated in brain, where aspartate *N*-acetyltransferase (Asp-NAT, encoded by the gene *Nat8l*) catalyzes the formation of NAA from acetyl-CoA and L-aspartate [20]. Thereafter, NAA is cleaved by aspartoacylase (*Aspa*) yielding L-aspartate and acetate. Subsequently, acetate can be incorporated into acetyl-CoA and acts as a precursor for lipid synthesis (*i.e.* myelination). Intact NAA metabolism has been shown to determine physiological function and status in the brain. Abnormalities in NAA levels have been reported in patients with cerebral disorders such as brain tumors, stroke, inborn genetic predispositions, and neurodegenerative disorders [21]. Although NAA metabolism has been studied mostly in the context of the central nervous system, several studies suggested an essential role of NAA in peripheral tissues and metabolic disorders [22–25]. For instance, Nat8l expression was significantly reduced in adipose depots of obese mice [19] and in subcutaneous and visceral fat of insulin-resistant obese humans [26].

Our previous studies showed that modulation of the NAA pathway impacts lipid metabolism [19,27]. Specifically, constitutive overexpression of Nat8l in brown adipocytes led to an increased incorporation of glucose into lipids [19], whereas blockage of the NAA pathway by knockdown of Aspa reduced cytosolic acetyl-CoA [27]. Interestingly, overexpression of Nat8l also caused increased lipolysis, brown marker gene expression, and mitochondrial respiration. In brown adipocytes, Nat8l is expressed in mitochondria [19], while Aspa is localized in the cytosolic fraction [27] indicating that NAA may act as a metabolic storage or transport molecule with the potential to modulate the availability of acetyl-CoA for lipid metabolism [28,29]. To better understand the observed phenotype and its relevance for brown adipocytes biology, we have investigated i) how the NAA pathway is physiologically regulated, ii) which energy sources are used for the formation of NAA, and iii) how manipulation of the NAA pathway impacts lipid metabolism and BAT biology.

2 Material and methods

2.1 Animal studies

All animal procedures were approved by the Austrian Ministry for Education, Science, and Research (Vienna, Austria) and were performed in accordance with these guidelines and regulations. Male C57BL/6J mice were used for this study. Animals were kept on a 14/10 h light/dark cycle and had *ad libitum* access to food and water, except when food was restricted during fasting. The fasting period was 24 h. At the age of 8–9 weeks, mice were either fed a chow diet (calories 11 kJ% from fat, 53 kJ% from carbohydrates, and 36 kJ% from protein, #V1126, Ssniff® Spezialdiäten, Soest, Germany) or put, at the age of 8–9 weeks on HGD (calories 7 kJ% from fat, 72 kJ% from carbohydrates, and 21 kJ% from protein, #E15629-34, Ssniff® Spezialdiäten, Soest, Germany) or on HFD (Sniff® Spezialdiäten, Soest, Germany, #E15744-34, 45 kJ% calories from fat, 35 kJ% from carbohydrates, and 20 kJ% from protein). Experiments were performed after 12–13 weeks (HGD) or 21–22 weeks (HFD) on the according diet (age and number of mice used are

noted in figure legends). Tissues were harvested from mice in fed *ad-libitum*, 24 h fasted or 2 h refed states after 24 h fasting and snap-frozen in liquid nitrogen.

2.2 Cell culture

To generate immortalized brown adipogenic cells (iBACs, obtained from Patrick Seale, University of Pennsylvania, USA), brown preadipocytes were isolated from newborn mice by collagenase digestion and immortalized by infection with the retroviral vector pBabe encoding SV40T antigen and selected with puromycin (2 μg/ml) [30]. Preadipocytes were grown to confluence in growth media (high glucose DMEM, #11995065) supplemented with 10% FBS, 50 μg/ml streptomycin, 50 units/ml penicillin, and 20 mM Hepes (all purchased from Thermo Fisher Scientific, Waltham, MA, USA) and were maintained at 37 °C and 5% CO_2. Adipocyte differentiation was induced by treating confluent cells for 48 h in differentiation medium (high glucose DMEM supplemented with 20 nM insulin, 1 nM triiodothyronine (T3), 0.5 mM 3-isobutyl-1-methylxanthine, 0.5 μM dexamethasone, and 0.125 mM indomethacin (all Merck, Darmstadt, Germany)). After a two-day induction period, the medium was replaced by growth medium supplemented with 20 nM insulin and 1 nM T3. Medium was changed every other day. Full differentiation was achieved after seven days. Stable overexpression of Nat8l in iBACs has been described elsewhere [19]. Nat8l knockdown cell lines were generated using lentiviral shRNA particles and a non-targeting control construct obtained from Merck (CSTVRS-TRCN0000114584, Merk, Darmstadt, Germany). Infected cells were selected with G418 (1.5 mg/ml, Roth, Karlsruhe, Germany) for seven days. To investigate autophagy flux by immunoblotting, fully differentiated brown adipocytes were cultivated in maintenance medium supplemented with bafilomycin A1 (100 nM 6 h, Merck, Darmstadt, Germany). Acetate complementation was performed supplementing 10 mM sodium acetate (Merck, Darmstadt, Germany), pH 7.4 to growth medium for 48 h. To determine lipolysis, free fatty acids were measured using NEFA-HR(2) Kit (Wako Chemicals, Osaka, Japan). Values were normalized to protein content (Pierce BCA reagent, Thermo Fisher Scientific, Waltham, MA, USA). To stimulate lipolysis, cells were incubated with 10 μM isoproterenol (Merck, Darmstadt, Germany) for 2 h. To determine effects of lipophagy or adipose triacylglycerol lipase (ATGL)-mediated lipolysis, cells were pretreated with 10 nM bafilomycin A1, 40 μM chloroquine (Merck, Darmstadt, Germany) or 40 μM atglistatin [31] (Ai) for 48 h. All cell lines were routinely monitored and confirmed to be free of mycoplasma.

2.3 Aspartoacylase activity assay

Differentiated iBACs (day 7 of differentiation) were harvested and samples prepared as described elsewhere [27]. The released aspartate content was analyzed using the aspartate assay kit (BioVision, Milpitas, CA, USA).

2.4 Cellular respiration

iBACs were plated in XF96 polystyrene cell culture microplates (Seahorse Bioscience®, Agilent, Santa Clara, CA, USA) at a density of 10,000 cells per well and differentiated to mature adipocytes. Pretreatment with inhibitors was performed for 2 h with the following concentrations: 40 μM atglistatin [31], 100 nM bafilomycin A1 (Merck, Darmstadt, Germany), and 40 μM chloroquine (Merck, Darmstadt, Germany). All inhibitors and 10 μM

Europe PMC Funders Author Manuscripts

isoproterenol (Merck, Darmstadt, Germany) were present during the 30 min equilibration in unbuffered XF assay medium (Seahorse Bioscience®, Agilent, Santa Clara, CA, USA) supplemented with 5.5–25 mM D-glucose, 2 mM glutamine and 1 mM sodium pyruvate at 37 °C in a non-CO_2 environment and during measurement. Oxygen consumption rate was subsequently measured every 7 min using an XF96 extracellular flux analyzer (Seahorse Bioscience, Agilent, Santa Clara, CA, USA). Optimal concentrations of specific inhibitors/accelerators of the electron transport chain were determined in a prior titration experiments and used as followed: 2 μM oligomycin, 0.3 μM carbonyl-cyanide *p*-trifluoromethoxyphenylhydrazone, 2.5 μM antimycin A (all reagents form Merck, Darmstadt, Germany). Results were normalized to protein concentration determined by BCA assay (Thermo Fisher Scientific, Waltham, MA, USA) and presented as pmol O_2/(min × μg protein).

2.5 Electron microscopy

High pressure freezing with a Leica EM HPM 100 (Leica Microsystems, Vienna, Austria) and freeze substitution: Cells were grown and differentiated on carbon coated sapphire discs. Discs were loaded and frozen using 2000 bar under liquid nitrogen conditions within milliseconds followed by freeze substitution in acetone by adding 2% osmium tetroxide and 0.2% uranyl acetate. After substitution, the samples were embedded in 100 epoxy resin (8 h), transferred into embedding moulds, and polymerized (48 h, 60 °C). Ultrathin sections (70 nm thick) were cut with a UC 7 Ultramicrotome (Leica Microsystems, Vienna, Austria) and stained with lead citrate for 5 min and platin blue for 15 min. Images were taken at 120 kV with a Tecnai G 2 FEI microscope equipped with an ultrascan 1000 ccd camera (Gatan, Pleasanton, CA, USA) [32]. Lysosomes were counted from all 90 electron micrographs from three biological replicates and related to total picture area.

2.6 Expression of mRFP-GFP-LC3 and confocal microscopy

Cells (day 5 of differentiation) and mRFP-GFP-LC3 (ptfLC3) plasmid (# 21074, Addgene plasmid Cambridge, MA, USA) were used for electroporation (EP) with the Neon® Transfection System (Thermo Fisher Scientific, Waltham, MA, USA) following the general protocol guidelines with the following modifications: iBACs were tryptic digested with 2.5% trypsin/0.5 U/ml collagenase D (Merck, Darmstadt, Germany) for 3.5 min and then resuspended in pre-warmed growth medium. Cells were pelleted at 300 ×*g* for 3 min and washed with PBS. Cells were counted and 450,000 cells and 2 μg plasmid DNA were mixed and used per 100 μl EP-tip. The EP was performed with the following program: 1400 V, 20 ms, 2 pulse and cells were plated on cover slides in 6-well plates in DMEM high glucose medium supplemented with FBS and without any antibiotics. The medium was changed to growth medium 24 h after EP and the cells (day 7 of differentiation) were subjected to confocal microscopy using a Leica HCX 63 × 1.25 NA water immersion objective on a Leica TCS SP5 confocal microscope (Leica Microsystems, Wetzlar, Germany).

2.7 HPLC/HRMS

2.7.1 Amino acid and TCA cycle intermediate detection—

To yield cellular metabolites, mature iBACs (cultivated in 6-well plates) were washed once with 10 mM

ammonium acetate buffer and washing solution was thoroughly removed before plates were frozen at −80 °C until measurement. For extraction, internal standard mix ($^{13}C_4$ NAA, $^{13}C_2$-acetyl-CoA) (Merck, Darmstadt, Germany) and yeast internal standard were added to each sample. Yeast internal standard mix (kind gift of Mario Klimacek, Graz University of Technology and HEALTH Institute for Biomedicine and Health Sciences, Joanneum Research, Graz, Austria) was generated as previously mentioned [33]. The extraction and HPLC method were used as previously described [27,34].

2.7.2 Determination of label incorporation into NAA—Isotopologue enrichment analysis to quantify the incorporation of [U-^{13}C]-glucose, [$^{13}C_5{}^{15}N_2$]-glutamine, [U-$^{13}C^{15}N$]-leucine + [U-$^{13}C^{15}N$]-valine, [U^{13}C]-acetate (Cambridge Isotope Laboratories, Tewksbury, MA, USA) into NAA was performed by liquid chromatography-mass spectrometry/high-resolution mass spectrometry (LC-MS/HRMS) using the method described by Guo et al. [35]. Immortalized brown adipocytes were grown in standard culture media DMEM 25 mM glucose, 10% dialyzed FBS without acetate, 1 mM sodium acetate, 4 mM glutamine, 20 mM HEPES, 100 U/ml penicillin, 100 g/ml streptomycin (Thermo Fisher Scientific Waltham, MA, USA), 1 nM T3, 20 nM insulin (Merck, Darmstadt, Germany) in 6 cm dishes. On day 6 of differentiation, media was replaced with tracing media (containing all components of the culture media except the unlabeled nutrient source replaced by either 25 mM [U-^{13}C]-glucose, 4 mM [$^{13}C_5{}^{15}N_2$]-glutamine, 0.8 mM [U-$^{13}C^{15}N$]-leucine + 0.8 mM [U-$^{13}C^{15}N$]-valine or 1 mM [U^{13}C]-acetate). Cells were incubated for 5 h in tracing media. Unlabeled cells were incubated in the same conditions in the absence of labeled substrate. At harvest, dishes were placed on ice, medium was aspirated thoroughly, cells were washed once with ice-cold PBS and immediately scraped into 1 ml/dish 80:20 MetOH:water pre-chilled to −80 °C. Samples were transferred to 1.5 ml tubes and pulse-sonicated for 30 s with a probe tip sonicator. Protein was precipitated over night at −20 °C, followed by centrifugation at 17,000 rcf at 4 °C for 10 min. The supernatant was transferred to glass tubes and dried under nitrogen. All samples were resuspended in 5% sulfosalicylic acid and 5 μl were injected for IP-RP-UPLC-MS (Thermo Fisher Scientific Waltham, MA, USA). Isotopologue enrichment in cells exposed to ^{13}C labeled substrates was calculated using unlabeled control samples as previously described [36].

2.7.3 Acyl-CoA quantitation—Internal standard generation: [$^{13}C_3{}^{15}N_1$]-labeled acyl-CoA internal standard was generated by culturing *pan6*-deficient *Saccharomyces cerevisiae* with [$^{13}C_3{}^{15}N_1$]-pantothenate (Isosciences, King of Prussia, PA, USA), as described previously by Snyder et al. [37]. A 500 ml culture at stationary phase was resuspended in 100 ml of 10% (w/v) trichloroacetic acid (Merck, Darmstadt, Germany cat. #T6399). The cells were dismembranated in 10 ml aliquots by sonication (60 pulses, 0.5 s) with a probe tip sonicator (Thermo Fisher Scientific, Waltham, MA, USA) and centrifuged at 3000*g* for 10 min at 4 °C. The cleared supernatant was stored at −80 °C. After incubation, cells were placed on ice, medium was aspirated completely and cells were harvested in 1 ml of ice-cold 10% trichloroacetic acid (Merck, Darmstadt, Germany, cat. #T6399). An equal volume of internal standard containing $^{13}C_3{}^{15}N_1$-labeled acyl-CoAs generated in *pan6*-deficient yeast culture [37] was added to each sample. Acyl-CoA thioester were analyzed by LC-MS/HRMS using an Ultimate 3000 autosampler coupled to a Thermo Q Exactive Plus

instrument in positive ESI mode using the settings described previously [38]. Acyl-CoA AUC values were normalized to the corresponding [$^{13}C_3{}^{15}N_1$]-labeled internal standard and protein concentration determined by Pierce BCA Kit (Thermo Fisher Scientific, Waltham, MA, USA).

2.8 Lysosomal acid lipase activity assay

Lysosomal acid lipase (LAL) activity was estimated using the fluorogenic substrate 4-methyl-umbelliferyl-palmitate (4-MUP) as described with some modifications [39]. Briefly, cells were harvested by trypsinization and the pellet was washed twice with ice cold PBS and stored at −80 °C until measurement. Afterwards, cell pellets were resolved in lysis buffer (100 mM $NaPO_4$, pH 6.8, 1 mM ethylenediaminetetraacetic acid, 10 mM dithiothreitol, 0.5% NP-40, 0.02% sodium azide, protease inhibitors) (Thermo Fisher Scientific, Waltham, MA, USA). Protein concentrations were quantified by a Lowry assay (Bio-Rad Laboratories, Hercules, CA, USA). Fifty microliters of 4-MUP substrate, 125 µl assay buffer (200 mM sodium acetate pH 4.5), and 25 µl cell lysate (containing 20 µg protein) were incubated for 2 h at 37 °C. The reaction was stopped by the addition of 100 µl of 0.75 M Tris (pH 11). Relative fluorescence units (RFU) were determined at 360 nm excitation/460 nm emission on a Victor 1420 multilabel counter (Per-kinElmer, Waltham, MA, USA) using 4-MU as standard. LAL activity is expressed as nmol MU/h * mg protein.

2.9 Lysosomal staining, flow cytometry, and confocal microscopy

Differentiated iBACs were stained with the fluorescent dye Lysotracker DeepRed (excitation/emission 647/668 nm) according to the manufacturer's protocol (Thermo Fisher Scientific, Waltham, MA, USA). Briefly, adipocytes were incubated for 30 min at 37 °C with 50 nM Lysotracker. Afterwards, cells were harvested and stained with Ghost Dye Red 780 (Tonbo Biosciences, San Diego, CA, USA) to exclude dead cells and subsequently washed three times with PBS detached with trypsin, centrifuged at 1200 rpm for 5 min, and resuspended in PBS. To quantify the number of lysosomes, 1×10^5 cells, gated for living cells, were analyzed using a Guava Easy Cyte 8 flow cytometer (Merck, Darmstadt, Germany). For confocal microscopy, cells were cultivated on cover slides in 6-well plates (Sarstedt, Nümbrecht, Germany) and stained with Lysotracker (described above). Afterwards, cells were imaged by confocal fluorescence microscopy using a Leica TCS SP5 confocal microscope (Leica Microsystems, Wetzlar, Germany) equipped with a Leica HCX 63 × 1.25 NA water immersion objective.

2.10 Microarray experiments and functional annotation

Total RNA from iBACs was isolated with PeqGOLD total RNA Isolation Kit (VWR, Darmstadt, Germany) according to manufacturer's recommendations. Two hundred nanograms of total RNA were prepared for Affymetrix hybridizations on Mouse Gene 2.0 ST Array. Raw array data were normalized using the RMA method implemented in CarmaWeb (https://carmaweb.genome.tugraz.at/carma/). For DAVID functional annotation, Ensembl Gene IDs of differentially regulated gene lists were submitted to the DAVID website [40]. KEGG pathways were considered significantly enriched if the Benjamini-Hochberg corrected p-value was < 0.05.

2.11 NMR metabolic profiling

Sample preparation and NMR measurements for ^{1}H NMR metabolic profiling were performed as previously described [41,42]. The 2D HSQC (heteronuclear single quantum correlation) pulse sequence (hsqcetgpsisp2, 8 scans, 256 points in F1, 2048 points in F2, 12,658.228 Hz spectral with in F1, 10,026.738 Hz spectral width in F2) was used for 2D ^{1}H-^{13}C experiments. Spectra pre-processing and statistical data analysis has been carried out using the state-of-the-art data analysis pipeline proposed by the group of Prof. Jeremy Nicholson at Imperials College London and using Matlab® scripts. NMR data were imported to Matlab® vR2014a (Mathworks, Natick, MA, USA), regions around the water, TSP, and remaining methanol signals excluded, and probabilistic quotient normalization was performed to correct for differences in sample metabolite dilution [43]. To identify changes in metabolic profiles, multivariate statistical analysis was performed. Statistical analysis includes Principle Component Analysis (PCA), Orthogonal Partial Least Squares Discriminant Analysis (O-PLS-DA), and all associated data consistency checks and 7-fold cross-validation [44]. Quantification for one-dimensional ^{1}H NMR spectra was performed using Chenomx NMR Suite 8.2 and for two-dimensional ^{1}H-^{13}C experiments spectral data were transferred to MestreNova 11.0.2 and processed (exponential line broadening of 0.3 Hz), phased, referenced to TSP and signals of interest were integrated.

2.12 Protein isolation and Western blotting analysis

Mature iBACs were harvested for protein analysis in SDS-lysis buffer 50 mM Tris-HCl, pH 6.8, 10% glycerol, 2.5% SDS (Merck, Darmstadt, Germany), 1× complete mini protease inhibitor cocktail (Roche, Basel, Switzerland) 1 mM phosphatase inhibitor PhosSTOP (Merck, Darmstadt, Germany). Nuclei fraction was isolated freshly from iBACs (approx. 10 × 10^{6} cells). Cell pellets were resuspended in 1 ml HES-buffer (20 mM HEPES, 1 mM EDTA, 250 mM sucrose; Merck, Darmstadt, Germany) containing 1× complete mini protease inhibitor cocktail (Roche, Basel, Switzerland) and 1 mM phosphatase inhibitor PhosSTOP (Merck, Darmstadt, Germany). Cell homogenization was performed using Dounce homogenizer. Cell debris (500 ×*g*, 5 min) were removed. The supernatant was centrifugation (1000 ×*g*, 10 min) to yield nuclei fraction. Nuclei pellets were resolved in SDS-lysis buffer. DNA and RNA in the cell lysates were digested with Benzonase® nuclease (Merck, Darmstadt, Germany). Thereafter, 20–30 μg of protein were subjected to 10% or 4–12% or 4–20% Bis-Tris NuPAGE gel (Thermo Fisher Scientific, Waltham, MA, USA), and gels were blotted to nitrocellulose membranes. The following antibodies were used either in Tris-buffered saline containing 0.05% Tween20 (TBST) or phosphatebuffered saline containing 0.05% Tween20 (PBST): anti-Asp-NAT (1:1000 in 5% BSA/TBST, kind gift of E. Van Schaftingen, Université Catholique de Louvain, Belgium), anti-ASPA (1:3000 in 5% BSA/TBST, GeneTex, GTX113389, Irvine, CA, USA), anti-AceCS1 (1:1000 in 5% BSA/TBST, Cell Signaling, #3658, Danvers, MA, USA), anti-GAPDH (1:1000 5% BSA/TBST, Cell Signaling, #2118, Danvers, MA, USA), anti-TFEB (1:2000 5% BSA/TBST, Bethyl Laboratories A303-673A, Montgomery, TX, USA), anti-phospho-S6 ribosomal protein (1:1000 in 5% BSA/TBST, Cell Signaling, #2211, Danvers, MA, USA), anti-histone H3 (1:1000 in 5% milk/TBST, Cell Signaling, #4499, Danvers, MA, USA), anti-LC3 (1:3000 in 5%milk, 1%BSA/TBST, Novus Biologicals, NB100-2220, Littleton, CO, USA), anti-UCP1 (1:750 in 1% BSA/TBST, Abcam, #ab10983, Cambridge, UK), and anti-β-actin (1:25,000 in

1% milk/PBST, Thermo Fisher Scientific, #A1978 Waltham, MA, USA). For chemiluminescence detection, a horseradish peroxidase-conjugated secondary antibody was used (anti-rabbit 1:2000; anti-mouse 1:3000, Agilent, Santa Clara, CA, USA). Amersham ECL Prime (Merck, Darmstadt, Germany) or Super Signal West Pico (Thermo Fisher Scientific, Waltham, MA, USA) served as substrates. β-Actin (ACTb), GAPDH or Ponceau S staining served as loading control.

2.13 RNA isolation, reverse transcription, and gene expression analysis

Cellular RNA was isolated using the PeqGOLD Total RNA Isolation Kit (VWR, Darmstadt, Germany). RNA from tissue was isolated using TRIzol reagent (Thermo Fisher Scientific, Waltham, MA, USA) according to the manufacturer's protocols. Reverse transcription for cDNA generation was performed using the QuantiTect Reverse Transcription Kit (Qiagen, Hilden, Germany). mRNA expression was assessed using real-time PCR using the StepOne Plus Detector system and SYBR Green PCR master mix (Thermo Fisher Scientific, Waltham, MA, USA). Gene expression was normalized to *TfIIβ* in cell lysates and *18s rRNA* in tissues. Relative mRNA expression levels were calculated using averaged 2^{-ddCt} values for each biological replicate [45]. For primer sequence, see Supplementary Table 1.

2.14 Statistical analysis

If not otherwise stated, results are shown as mean ± SD of at least three biological replicates or results show one representative experiment out of three. Statistical analysis was performed on all available data. Statistical significance was determined using the unpaired two-tailed Student's *t*-test and defined as $*p < 0.05$; $**p < 0.01$; $***p < 0.001$, $****p < 0.001$.

3 Results

3.1 The NAA pathway is regulated by glucose and nutrient availability in adipose tissue

Adipocytes play a key role in the maintenance of whole-body energy homeostasis by sensing nutrient availability and adapting metabolic gene expression [46]. To investigate a potential role of the NAA pathway in metabolic adaptation in adipose tissue (AT), we examined the mRNA expression of the key enzymes in NAA metabolism (*Nat8l* and *Aspa*) under different physiological conditions. To that end, C57BL/6J mice were fed *ad libitum*, fasted for 24 h or refed for 2 h after fasting. In BAT and epididymal white adipose tissue (eWAT), *Nat8l* and *Aspa* expression declined with fasting and returned to baseline after 2 h of refeeding a chow diet (Fig. 1A, B). This regulation is in accordance with genes involved in glucose metabolism and *de novo* lipogenesis (DNL) (Fig. S1A). Further, we investigated mRNA expression of NAA pathway genes in BAT under nutrient-rich conditions mimicked by high-glucose diet (HGD) and high-fat diet (HFD) feeding. On these energy-rich diets, *Nat8l* and *Aspa* expression (Fig. 1C, D) as well as control genes involved in glucose metabolism and lipogenesis (Fig. S1B, C) were increased when compared to mice fed a chow diet. To determine whether alterations in glucose availability selectively regulate *Nat8l* or *Aspa*, we examined their expression in immortalized brown adipogenic cells (iBACs). Glucose depletion strongly decreased *Nat8l* and *Aspa* expression and replenishment of glucose completely restored expression of both genes (Fig. 1E). A similar response to changes in

glucose flux was seen in the expression of glucose-regulated genes (Fig. S1D). As expected from elevated *Nat8l* expression in mature adipocytes compared to pre-adipocytes [19], NAA levels also strongly increased upon differentiation of iBACs (Fig. 1F).

To identify the key substrates used for NAA production, we cultured iBACs in growth media with uniformly labeled ^{13}C-glucose, ^{13}C-acetate or ^{13}C- and ^{15}N-labeled glutamine or branched-chain amino acids (BCAA), namely leucine and valine. Incorporation of heavy isotope label into NAA and its precursor molecules, acetyl-CoA and aspartate was examined by mass spectrometry (Fig. 1G, H). The relative abundance of isotopic carbon labels revealed the preferential utilization of glucose for NAA production in iBACs (Fig. 1H). Glucose was the only substrate that labeled all six carbon atoms of NAA (M + 6) and was the major contributor to M + 2, M + 3, M + 4, and M + 5 NAA, suggesting that glucose supplies both acetyl-CoA and L-aspartate for NAA synthesis (Fig. 1H, I). Interestingly, BCAA (leucine and valine) and glutamine contributed to NAA labeling by supplying their amino group (Fig. 1H, Fig. S1E). In comparison to glucose, the carbon contribution from BCAA, glutamine, and acetate was minimal (Fig. 1H). Taken together, expression of *Nat8l* and *Aspa* are nutritionally regulated and respond robustly to changes in glucose availability. NAA is preferentially produced from glucose-derived acetyl-CoA and aspartate and increases during adipogenesis, suggesting that NAA might be an essential contributor to the adipocyte energy metabolite pool.

3.2 NAA pathway activity affects metabolic pathways, lipid and energy metabolism

Our data revealed that *Nat8l* expression is increased under nutrientrich conditions and upon BAT activation [27]. To further investigate the role of *Nat8l* in energy metabolism and metabolic pathways of brown adipocytes, we overexpressed *Nat8l* in iBACs (Nat8l o/e). As expected, we detected increased *Nat8l* mRNA and Asp-NAT protein expression (Fig. 2A, B). In addition, Nat8l o/e resulted in coordinated up-regulation of pathway enzymes, including ASPA and acyl-CoA synthetase short-chain family member 2 (ACSS2), which are responsible for NAA cleavage to acetate and aspartate and converting acetate into acetyl-CoA, respectively (Fig. 2B). Furthermore, we observed increased ASPA activity, which enables an increased flux through the NAA pathway (Fig. 2C).

Transcriptomics analysis followed by DAVID functional clustering on the set of genes upregulated by Nat8l o/e revealed an enrichment of genes involved in metabolic pathways, such as oxidative phosphorylation, carbon metabolism, TCA cycle, FA degradation and metabolic processes, degradation of BCAAs and FA elongation (Fig. 2D), indicating that *Nat8l* is involved in the regulation of BAT metabolism. This prompted us to investigate the effect of Nat8l o/e on cellular metabolism in more details. Metabolic profiling showed significantly elevated NAA levels upon Nat8l o/e (Fig. 2E). As labeling experiments revealed glucose as the main contributor to NAA synthesis in brown adipocytes, we performed untargeted ^{13}C-glucose tracing in control and Nat8l o/e iBACs. We observed a dynamic formation of NAA over a time course of 8 h. In Nat8l o/e cells, we detected increased incorporation of ^{13}C glucose-derived acetyl-CoA into NAA compared to control cells (Fig. 2F). Concomitantly, unlabeled (^{12}C) NAA decreased over time, suggesting an active turnover of NAA (Fig. 2G). However, the percent label enrichment from ^{13}C labeled

glucose, acetate, BCAA or glutamine was comparable between control and Nat8l o/e iBACs revealing that the overexpression did not alter the way NAA was synthesized and also Nat8l o/e iBACs used glucose as their main source (Fig. S2A).

We hypothesized that increased NAA metabolism might shuttle acetyl-CoA to the cytosol, where it serves as precursor for lipid synthesis. Therefore, we investigated cytoplasmic intermediates of neutral lipid (malonyl-CoA) and cholesterol (3-hydroxy-3-methylglutaryl-CoA, HMG-CoA) biosynthesis. Our data revealed that malonyl-CoA (Fig. 2H) and HMG-CoA (Fig. 2I) were more abundant in Nat8l o/e iBACs, which is consistent with our previous findings that Nat8l o/e promotes DNL. Further investigation of the impact of increased Asp-NAT activity on energy metabolism with ^{13}C-glucose tracing revealed that glucose-derived TCA cycle intermediates such as citrate and malate were reduced (Fig. 2J, K). In addition, increased AA catabolism has been detected. Specifically, we observed a significant reduction of arginine, glutamine, glycine, threonine, tryptophan, leucine, lysine and valine and a significant increase of aspartate (Fig. 2L, M). In summary, these data provide evidence that increased Asp-NAT expression accelerates the entire NAA pathway and impacts metabolic pathways and energy metabolism.

3.3 Increased NAA pathway activity elevates the number of lysosomes and induces autophagy

To identify the mechanisms of altered energy metabolism and increased lipid turnover [19] upon increased NAA pathway activity, we tested the hypothesis that maintenance of energy homeostasis requires the induction of autophagy. Autophagy is a catabolic process that degrades cellular components within autophagolysosomes and plays a particularly critical role in recycling metabolites [47]. Transcription factor EB (TFEB) translocation to the nucleus and activates the expression of genes involved in autophagy and lysosomal biogenesis [48]. To address TFEB translocation, we performed subcellular fractionation and found increased TFEB in the nucleus upon Nat8l o/e (Fig. 3A). Concomitantly, we counted elevated number of lysosomes, as determined by transmission electron microscopy (Fig. 3B, C). Additionally, incubation of cell with the fluorescence dye LysoTracker, which stains acidic compartments (lysosomes) in living cells, and subsequent analysis by fluorescence microscopy and quantification using flow cytometry revealed a two-fold increase in the number of lysosomes (Fig. 3D, E). Furthermore, we observed increased protein levels of the autophagy marker LC3-II under basal conditions and after treatment with the autophagy inhibitor bafilomycin A1 (BafA1) (Fig. 3F). To further corroborate these findings, we transfected cells with the tandem mRFP-GFP-LC3 sensor that contains an acid-stable RFP and acid-labile GFP to distinguish between autophagosome and autolysosome by confocal microscopy [49]. We observed that Nat8l o/e increased the number of autophagosomes and autolysosomes, detected by an increase of red vesicles (mRFP-positive), but not green vesicles (as the GFP signal is quenched in the acidic lysosomal environment), indicating an increased autophagic flux (Fig. 3G). To address if the increased requirement of acetyl-CoA for NAA synthesis drives the increased induction of autophagy, we aimed to replenish acetyl-CoA and to monitor LC3-II expression. Of note, autophagic levels of Nat8l o/e cells returned to baseline control levels in response to acetate supplementation (Fig. 3H, I). Together, these data suggest that Nat8l o/e activates autophagy as a compensatory pathway

to maintain energy homeostasis as evident by increased lysosomal content and autophagy flux.

3.4 Increased lipid catabolism and cellular respiration in Nat8l o/e iBACs are lipophagy and ATGL-mediated

Our recent publication showed that flux through the NAA pathway affects brown adipocytes by increasing free FA turnover and oxygen consumption rate (OCR) in Nat8l o/e iBACs [19]. FAs are important energy substrates and activate peroxisome proliferator-activated receptor (PPAR)α and PPARα target gene expression and thereby mitochondrial respiratory functions [4,50]. Hence, we investigated whether the elevated number of lysosomes and autophagolysosomes contribute to this increased free FA release *via* the process of lipophagy. We detected increased activity of LAL, which is active at an acidic pH and mediates lysosomal degradation of lipids (Fig. 4A). In line, inhibition of autophagy flux by BafA1 (Fig. 4B) and chloroquine (CQ) (Fig. 4C) significantly reduced free FA release in control and Nat8l o/e cells. Importantly, autophagy inhibition was sufficient to reduce free FA release of Nat8l o/e cells to control levels (Fig. 4B, C). In addition, chemical inhibition of ATGL by atglistatin (Ai) strikingly reduced free FA release (Fig. 4D). To determine the relative contribution of acid and neutral lipolysis to increased OCR observed upon Nat8l o/e in iBACs, we compared basal and uncoupled respiration of control and Nat8l o/e iBACs upon autophagy and neutral lipolysis inhibition. BafA1 (Fig. 4E–G), CQ (Fig. 4H–J) as well as Ai (Fig. 4K–M) treatment blocked Nat8l o/e-induced basal and maximum respiration. In line with these results, activation of neutral lipolysis by isoproterenol (Iso) increased free FA release (Fig. S3A) and further induced basal and maximum respiration (Fig. S3B–D). Together, these data indicate that a combined activation of neutral and acid lipolysis is responsible for the increased lipid catabolism and supports the elevated mitochondrial respiration in Nat8l o/e iBACs.

3.5 Impact of Nat8l knockdown on energy metabolism, lysosomal biogenesis, and autophagy

Finally, we investigated the influence of lentiviral shRNA-mediated *Nat8l* knockdown (Nat8l-KD) on energy metabolism and autophagy in iBACs. We achieved a strong KD of *Nat8l* accompanied by downregulation of *Aspa* and *Acss2* mRNA and Asp-NAT, ASPA and ACSS2 protein expression (Fig. 5A, B). Corroborating effective Nat8l-KD, metabolites directly involved in the NAA pathway, such as NAA and aspartate, were significantly reduced (Fig. 5C, D), whereas TCA cycle intermediates and BCAA were unaffected (Fig. 5E, F). Apart from reduced glutamine and increased proline levels, AA levels were unchanged upon Nat8l-KD (Fig. 5G). In contrast to increased lysosomal number and autophagy in Nat8l o/e cells, Nat8l-KD showed reduced number of lysosomes and trends to decreased abundance of LC3-II in the absence and presence of BafA1 (Fig. 5H–J). Together, the data suggests that Asp-NAT is the primary enzyme responsible for the biosynthesis of NAA in brown adipocytes and coordinates the entire pathway. Inhibition of NAA synthesis might make more acetyl-CoA available for other metabolic pathways and therefore lysosomal degradation and autophagy are not required.

4 Discussion

This study uncovers the NAA pathway as a new nutrient-responsive player in the regulation of energy metabolism in adipose tissue (AT). Recently, we and others reported a crucial role for NAA outside the CNS [22–25,51]. Here, we provide evidence that a continuous supply with dietary nutrients is a prerequisite for the activation of the NAA pathway in AT and nutrient-rich conditions (HGD, HFD) further upregulate this pathway. Specifically, high glucose availability acts as a potent trigger to regulate *Nat8l* and *Aspa* gene expression in brown adipocytes. Of note, increased glucose uptake during adipogenesis [15] might explain the upregulation of the NAA pathway genes and NAA levels upon differentiation. The feeding/fasting response of the NAA pathway is in accordance with clinical data, which showed that NAA concentrations were blunted in brain during energy-demanding processes such as hypoxia as well as after stroke and traumatic brain injury [52–54]. In addition, we have previously shown that *Nat8l* expression was downregulated in BAT and eWAT of genetically obese (ob/ob) mice [19]. Of note, ob/ob mice are diabetic and highly insulin-resistant. Thus, decreased glucose uptake resulting from AT insulin resistance might be an explanation for decreased *Nat8l* expression in ob/ob mice. Consistently, NAA concentrations in serum and urine of ob/ob mice were reduced [55]. In this study, we identified glucose as the main substrate for NAA synthesis in brown adipocytes, indicating a direct link between glucose availability and NAA synthesis.

Our study revealed that increased NAA pathway activity altered energy metabolism in brown adipocytes and interfered with lipid metabolism. We observed increased incorporation of ^{13}C glucose-derived acetyl-CoA into NAA upon Nat8l o/e. Our data suggest that an increased requirement of acetyl-CoA for NAA synthesis might activate compensatory mechanisms such as acid lipolysis, leading to increased TFEB translocation to the nucleus, increased lysosomal biogenesis, and elevated LC3 lipidation. These findings are further supported by our previous study, where we demonstrated elevated expression of several TFEB target genes such as PGC1α and PPARα, which mediate mitochondrial biogenesis and oxidative phosphorylation [19]. Increased number of lysosomes, elevated autophagic flux, and increased activity of LAL indicate that specifically lipid degradation by lipophagy might be induced in Nat8l o/e iBACs to maintain energy homeostasis. Concomitantly, we found a substantial contribution of ATGL-mediated lipolysis to TG degradation. Although the interplay between lipophagy and lipolysis has not been resolved yet, it was suggested that lipophagy complements neutral lipolysis and that they regulate each other. Both lipophagy and lipolysis hydrolyze LD-stored TGs and deliver FA, which support OCR and browning [4]. Our data indicate that activation of acid and neutral lipolysis contributed to increased lipid catabolism in Nat8l o/e iBACs and elevated mitochondrial respiration was also largely dependent on the increased lipolytic activity.

Apart from the induction of neutral and acid lipolysis, Nat8l o/e iBACs showed increased L-aspartate and NAA levels. *Vice versa*, we observed reduced L-aspartate concentrations accompanied by a strong reduction of NAA in Nat8l-KD cells, indicating a regulation of the aspartate pool through modulated NAA pathway activity. So far it is unknown if NAA-derived aspartate (as a result of ASPA-mediated hydrolysis), is utilized for protein synthesis and cell proliferation or whether it re-enters the TCA cycle as oxaloacetate for energy

derivation. The regulation of the aspartate pool by the NAA pathway might be also relevant in the context of cancer. Interestingly, non small cell lung cancer cells with metabolic abnormalities, including elevated NAA levels, synthesize the aspartate moiety of NAA predominantly from glutamine [22]. However, some cancer types including ovarian cancer show elevated glucose uptake and utilization [56,57] and high levels of NAA and its biosynthetic enzyme Asp-NAT [22]. In line, we identified glucose as the main source for NAA synthesis in brown adipocytes. These findings suggest that the NAA pathway is differently regulated in various tissues and upon pathophysiological conditions.

In conclusion, our data contribute to the understanding how the NAA pathway increases energy expenditure in brown adipocytes. We demonstrate that nutrient availability and specifically exogenous glucose activate the NAA pathway. NAA is preferentially produced from glucose-derived acetyl-CoA and aspartate. Elevated NAA pathway activity upon overexpression of Nat8l drains glucose-derived acetyl-CoA into the NAA pool thereby affecting lipid turnover, AA degradation and TCA cycle intermediates. We conclude that the NAA pathway is an important regulator of nutrient availability and energy homeostasis in brown adipocytes. Therefore, we suggest the NAA pathway as a promising target to combat metabolic complications associated with adipose tissue dysfunction.

Supplementary Material

Refer to Web version on PubMed Central for supplementary material.

Acknowledgements

This work was supported by the Austrian Science Fund FWF [DK-MCD W1226, P24143, P27108, and P27070]. The authors gratefully acknowledge support from NAWI Graz. We thank Thomas Schreiner, Wolfgang Krispel and Dominique Pernitsch for excellent technical assistance and J.G. B.-S. and K.E.W. group members for helpful discussions during the preparation of the manuscript.

References

[1]. González-Muniesa P, et al. Obesity. Nat Rev Dis Primer. 2017; 3:17034.

[2]. Yoneshiro T, et al. Recruited brown adipose tissue as an antiobesity agent in humans. J Clin Invest. 2013; 123:3404–3408. [PubMed: 23867622]

[3]. Townsend KL, Tseng Y-H. Brown fat fuel utilization and thermogenesis. Trends Endocrinol Metab TEM. 2014; 25:168–177. [PubMed: 24389130]

[4]. Zechner R, Madeo F, Kratky D. Cytosolic lipolysis and lipophagy: two sides of the same coin. Nat Rev Mol Cell Biol. 2017; 18:671–684. [PubMed: 28852221]

[5]. Calderon-Dominguez M, et al. Fatty acid metabolism and the basis of brown adipose tissue function. Adipocyte. 2015; 5:98–118. [PubMed: 27386151]

[6]. Zimmermann R, et al. Fat mobilization in adipose tissue is promoted by adipose triglyceride lipase. Science. 2004; 306:1383–1386. [PubMed: 15550674]

[7]. Villena JA, Roy S, Sarkadi-Nagy E, Kim K-H, Sul HS, et al. J Biol Chem. 2004; 279:47066–47075. [PubMed: 15337759]

[8]. Jenkins CM, et al. Identification, cloning, expression, and purification of three novel human calcium-independent phospholipase A2 family members possessing triacylglycerol lipase and acylglycerol transacylase activities. J Biol Chem. 2004; 279:48968–48975. [PubMed: 15364929]

[9]. Vaughan M, Berger JE, Steinberg D. Hormone-sensitive lipase and monoglyceride lipase activities in adipose tissue. J Biol Chem. 1964; 239:401–409. [PubMed: 14169138]

[10]. Martinez-Lopez N, et al. Autophagy in the CNS and periphery coordinate lipophagy and lipolysis in the brown adipose tissue and liver. Cell Metab. 2016; 23:113–127. [PubMed: 26698918]

[11]. Cingolani F, Czaja MJ. Regulation and functions of autophagic lipolysis. Trends Endocrinol Metab TEM. 2016; 27:696–705. [PubMed: 27365163]

[12]. Singh R, et al. Autophagy regulates lipid metabolism. Nature. 2009; 458:1131–1135. [PubMed: 19339967]

[13]. Sheriff S, Du H, Grabowski GA. Characterization of lysosomal acid lipase by site-directed mutagenesis and heterologous expression. J Biol Chem. 1995; 270:27766–27772. [PubMed: 7499245]

[14]. Warner TG, Dambach LM, Shin JH, O'Brien JS. Purification of the lysosomal acid lipase from human liver and its role in lysosomal lipid hydrolysis. J Biol Chem. 1981; 256:2952–2957. [PubMed: 7204383]

[15]. Cannon B, Nedergaard J. Brown adipose tissue: function and physiological significance. Physiol Rev. 2004; 84:277–359. [PubMed: 14715917]

[16]. Leitner BP, et al. Mapping of human brown adipose tissue in lean and obese young men. Proc Natl Acad Sci U S A. 2017; 114:8649–8654. [PubMed: 28739898]

[17]. Loyd C, Obici S. Brown fat fuel use and regulation of energy homeostasis. Curr Opin Clin Nutr Metab Care. 2014; 17:368–372. [PubMed: 24839950]

[18]. Nakamura Y, Nakamura K. Central regulation of brown adipose tissue thermogenesis and energy homeostasis dependent on food availability. Pflugers Arch. 2018; 470:823–837. [PubMed: 29209779]

[19]. Pessentheiner AR, et al. NAT8L (N-acetyltransferase 8-like) accelerates lipid turnover and increases energy expenditure in brown adipocytes. J Biol Chem. 2013; 288:36040–36051. [PubMed: 24155240]

[20]. Goldstein FB. Biosynthesis of N-acetyl-L-aspartic acid. Biochim Biophys Acta. 1959; 33:583–584. [PubMed: 13670942]

[21]. Mehta V, Namboodiri MA. N-acetylaspartate as an acetyl source in the nervous system. Brain Res Mol Brain Res. 1995; 31:151–157. [PubMed: 7476023]

[22]. Lou T-F, et al. Cancer-specific production of N-acetylaspartate via NAT8L over-expression in non-small cell lung cancer and its potential as a circulating biomarker. Cancer Prev Res Phila Pa. 2016; 9:43–52.

[23]. Wynn ML, et al. RhoC GTPase is a potent regulator of glutamine metabolism and N-acetylaspartate production in inflammatory breast cancer cells. J Biol Chem. 2016; 291:13715–13729. [PubMed: 27129239]

[24]. Zand B, et al. Role of increased n-acetylaspartate levels in cancer. J Natl Cancer Inst. 2016; 108:djv426. [PubMed: 26819345]

[25]. Weindl D, et al. Bridging the gap between non-targeted stable isotope labeling and metabolic flux analysis. Cancer Metab. 2016; 4

[26]. Hardy OT, et al. BMI-independent inflammation in omental adipose tissue associated with insulin resistance in morbid obesity. Surg Obes Relat Dis Off J Am Soc Bariatr Surg. 2011; 7:60–67.

[27]. Prokesch A, et al. N-acetylaspartate catabolism determines cytosolic acetyl-CoA levels and histone acetylation in brown adipocytes. Sci Rep. 2016; 6:23723. [PubMed: 27045997]

[28]. Patel TB, Clark JB. Synthesis of N-acetyl-L-aspartate by rat brain mitochondria and its involvement in mitochondrial/cytosolic carbon transport. Biochem J. 1979; 184:539–546. [PubMed: 540047]

[29]. Patel TB, Clark JB. Lipogenesis in the brain of suckling rats. Studies on the mechanism of mitochondrial-cytosolic carbon transfer. Biochem J. 1980; 188(1):163–168. [PubMed: 7406877]

[30]. Harms MJ, et al. Prdm16 is required for the maintenance of brown adipocyte identity and function in adult mice. Cell Metab. 2014; 19:593–604. [PubMed: 24703692]

[31]. Schweiger M, et al. Pharmacological inhibition of adipose triglyceride lipase corrects high-fat diet-induced insulin resistance and hepatosteatosis in mice. Nat Commun. 2017; 8

[32]. Studer D, Humbel BM, Chiquet M. Electron microscopy of high pressure frozen samples: bridging the gap between cellular ultrastructure and atomic resolution. Histochem Cell Biol. 2008; 130:877–889. [PubMed: 18795316]

[33]. Mashego MR, et al. MIRACLE: mass isotopomer ratio analysis of U-13C-labeled extracts. A new method for accurate quantification of changes in concentrations of intracellular metabolites. Biotechnol Bioeng. 2004; 85:620–628. [PubMed: 14966803]

[34]. Ritter JB, Genzel Y, Reichl U. Simultaneous extraction of several metabolites of energy metabolism and related substances in mammalian cells: optimization using experimental design. Anal Biochem. 2008; 373:349–369. [PubMed: 18036549]

[35]. Guo L, et al. Diisopropylethylamine/hexafluoroisopropanol-mediated ion-pairing ultra-high-performance liquid chromatography/mass spectrometry for phosphate and carboxylate metabolite analysis: utility for studying cellular metabolism. Rapid Commun Mass Spectrom RCM. 2016; 30:1835–1845. [PubMed: 27476658]

[36]. Trefely S, Ashwell P, Snyder NW. FluxFix: automatic isotopologue normalization for metabolic tracer analysis. BMC Bioinforma. 2016; 17

[37]. Snyder NW, et al. Production of stable isotope-labeled acyl-coenzyme A thioesters by yeast stable isotope labeling by essential nutrients in cell culture. Anal Biochem. 2015; 474:59–65. [PubMed: 25572876]

[38]. Frey AJ, et al. LC-quadrupole/Orbitrap high resolution mass spectrometry enables stable isotope resolved simultaneous quantification and 13C-isotopic labeling of acyl-coenzyme A thioesters. Anal Bioanal Chem. 2016; 408:3651–3658. [PubMed: 26968563]

[39]. Schlager S, et al. Lysosomal lipid hydrolysis provides substrates for lipid mediator synthesis in murine macrophages. Oncotarget. 2017; 8:40037–40051. [PubMed: 28402950]

[40]. Huang DW, et al. The DAVID gene functional classification tool: a novel biological module-centric algorithm to functionally analyze large gene lists. Genome Biol. 2007; 8:R183. [PubMed: 17784955]

[41]. Radović B, et al. Lysosomal acid lipase regulates VLDL synthesis and insulin sensitivity in mice. Diabetologia. 2016; 59:1743–1752. [PubMed: 27153842]

[42]. Prokesch A, et al. Liver p53 is stabilized upon starvation and required for amino acid catabolism and gluconeogenesis. FASEB J Off Publ Fed Am Soc Exp Biol. 2017; 31:732–742.

[43]. Dieterle F, Ross A, Schlotterbeck G, Senn H. Probabilistic quotient normalization as robust method to account for dilution of complex biological mixtures. Application in 1H NMR metabonomics. Anal Chem. 2006; 78:4281–4290. [PubMed: 16808434]

[44]. Maher AD, et al. Optimization of human plasma 1H NMR spectroscopic data processing for high-throughput metabolic phenotyping studies and detection of insulin resistance related to type 2 diabetes. Anal Chem. 2008; 80:7354–7362. [PubMed: 18759460]

[45]. Livak KJ, Schmittgen TD. Analysis of relative gene expression data using real-time quantitative PCR and the 2(−delta dselta C(T)) method. Methods San Diego Calif. 2001; 25:402–408.

[46]. Attie AD, Scherer PE. Adipocyte metabolism and obesity: fig. 1. J Lipid Res. 2009; 50:S395–S399. [PubMed: 19017614]

[47]. Rabinowitz JD, White E. Autophagy and metabolism. Science. 2010; 330:1344–1348. [PubMed: 21127245]

[48]. Settembre C, et al. TFEB links autophagy to lysosomal biogenesis. Science. 2011; 332:1429–1433. [PubMed: 21617040]

[49]. Sathyanarayan A, Mashek MT, Mashek DG. ATGL promotes autophagy/lipophagy via SIRT1 to control hepatic lipid droplet catabolism. Cell Rep. 2017; 19:1–9. [PubMed: 28380348]

[50]. Zierler KA, et al. Functional cardiac lipolysis in mice critically depends on comparative gene identification-58. J Biol Chem. 2013; 288:9892–9904. [PubMed: 23413028]

[51]. Bogner-Strauss JG. N-acetylaspartate metabolism outside the brain: lipogenesis, histone acetylation, and cancer. Front Endocrinol. 2017; 8:240.

[52]. Fenstermacher MJ, Narayana PA. Serial proton magnetic resonance spectroscopy of ischemic brain injury in humans. Investig Radiol. 1990; 25:1034–1039. [PubMed: 2211046]

[53]. Moffett JR, Arun P, Ariyannur PS, Namboodiri AMA. N-acetylaspartate reductions in brain injury: impact on post-injury neuroenergetics, lipid synthesis, and protein acetylation. Front Neuroenerg. 2013; 5

[54]. Signoretti S, et al. N-acetylaspartate reduction as a measure of injury severity and mitochondrial dysfunction following diffuse traumatic brain injury. J Neurotrauma. 2001; 18:977–991. [PubMed: 11686498]

[55]. Won E-Y, et al. Gender-specific metabolomic profiling of obesity in leptin-deficient ob/ob mice by 1H NMR spectroscopy. PLoS One. 2013; 8:e75998. [PubMed: 24098417]

[56]. Rudlowski C, Moser M, Becker AJ, Rath W, Buttner R, Schroder W, Schurmann A. GLUT1 mRNA and protein expression in ovarian borderline tumors and cancer. Oncology. 2004; 66:404–410. [PubMed: 15331928]

[57]. Wang J, Ye C, Chen C, Xiong H, Xie B, Zhou J, Chen Y, Zheng S, Wang L. Glucose transporter GLUT1 expression and clinical outcome in solid tumors: a systematic review and meta-analysis. Oncotarget. 2017; 8:16875–16886. [PubMed: 28187435]

Europe PMC Funders Author Manuscripts

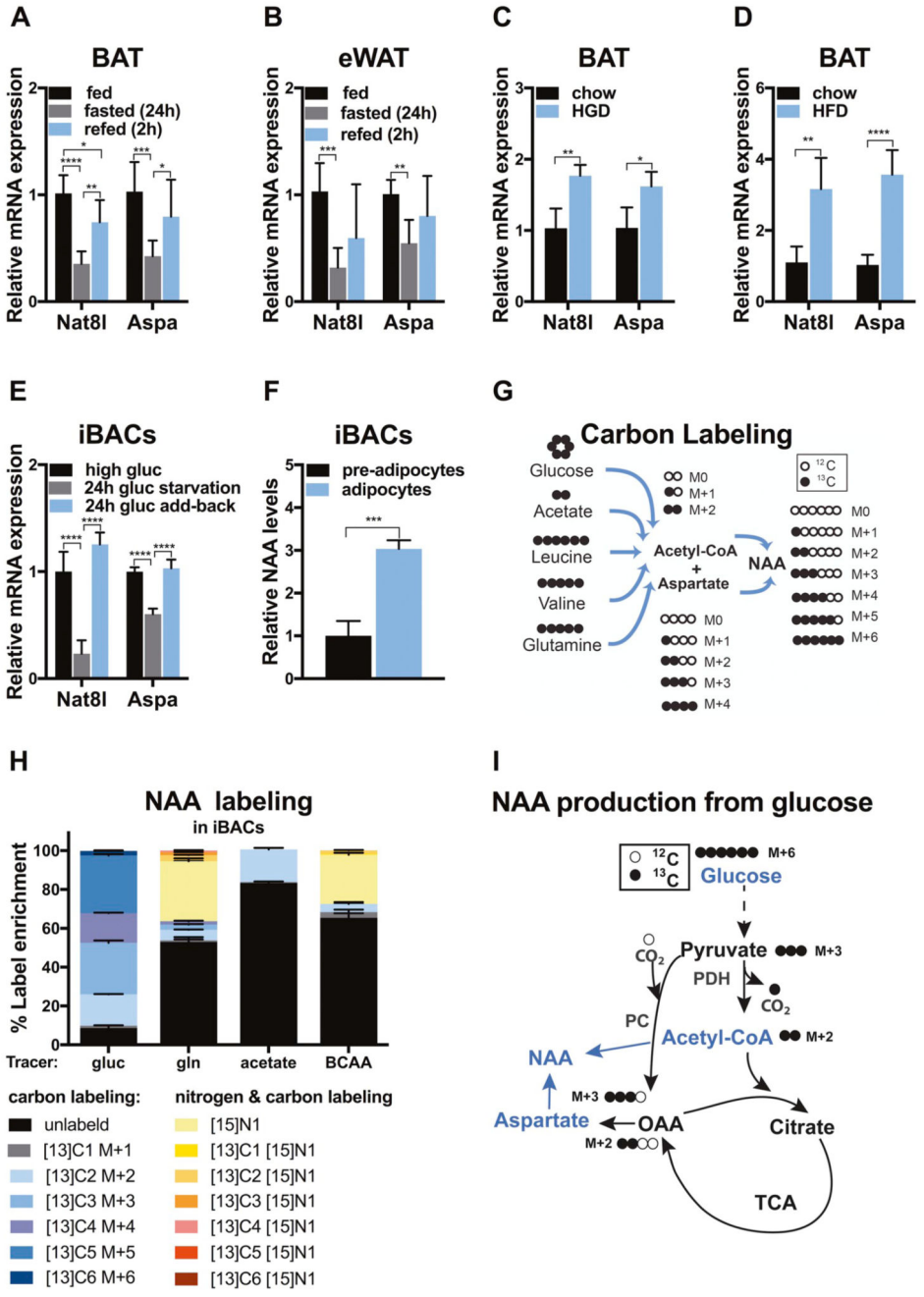

Fig. 1. The NAA pathway is regulated in a glucose and nutrient-dependent manner.

Quantitative real-time PCR analysis of *Nat8l* and *Aspa* mRNA expression in (A) brown adipose tissue (BAT) and (B) epididymal white adipose tissue (eWAT) isolated from male, 12-week-old C57BL/6J mice fed chow diet *ad libitum*, 24 h fasted, or 2 h refed a chow after 24 h fasting ($n = 5$). (C) BAT from 20-week-old mice harvested in overnight fasted – 2 h refed state. Mice were fed a chow or high-glucose diet (HGD). HGD started at the age of 8 weeks ($n = 4$). (D) BAT from 29-week-old mice harvested in fed state. Mice were fed chow or high-fat diet (HFD). HFD started at the age of 8 weeks ($n = 5$). (E) *Nat8l* and *Aspa*

Europe PMC Funders Author Manuscripts

mRNA expression in mature immortalized brown adipogenic cells (iBACs) cultivated in high-glucose (gluc) media, 24 h depleted from gluc or 24 h of gluc replenishment after 24 h of gluc depletion, ($n = 4$). (F) Relative NAA levels in brown pre-adipocytes and mature iBACs cultivated in high gluc medium ($n = 3$). (G) Schematic depicting experimental design of NAA carbon labeling produced from acetyl-CoA and aspartate using either [U-^{13}C]-gluc, [1,2-$^{13}C_2$]-acetate, branched chain amino acids (BCAA) such as [$^{13}C_6$,^{15}N]-L-leucine and [$^{13}C_5$,^{15}N]-L-valine or [$^{13}C_5$,$^{15}N_2$]-L-glutamine (gln). M + n: a metabolite with n carbon atoms labeled with ^{13}C. (H) iBACs were cultured 5 h in the presence of indicated tracer followed by mass spectrometry. The color codes indicate for the percentage of carbon and nitrogen incorporated into NAA that is heavy isotope-labeled by the indicated number of n atoms labeled with ^{13}C ($n = 3$). (I) NAA labeling scheme using [U-^{13}C]-gluc. For simplicity, labeling of only the first round of TCA cycle is shown. Oxaloacetic acid (OAA) is produced from pyruvate *via* pyruvate carboxylation (PC) or pyruvate dehydrogenase (PDH) yielding acetyl-CoA, which enters the TCA cycle. Aspartate is synthesized through the transamination of OAA. Data are shown as mean ± SD. Statistical significance was calculated using two-tailed Student's *t*-test (*$p < 0.05$, **$p < 0.01$, ***$p < 0.001$, ****$p < 0.0001$). (For interpretation of the references to color in this figure legend, the reader is referred to the web version of this article.)

Europe PMC Funders Author Manuscripts

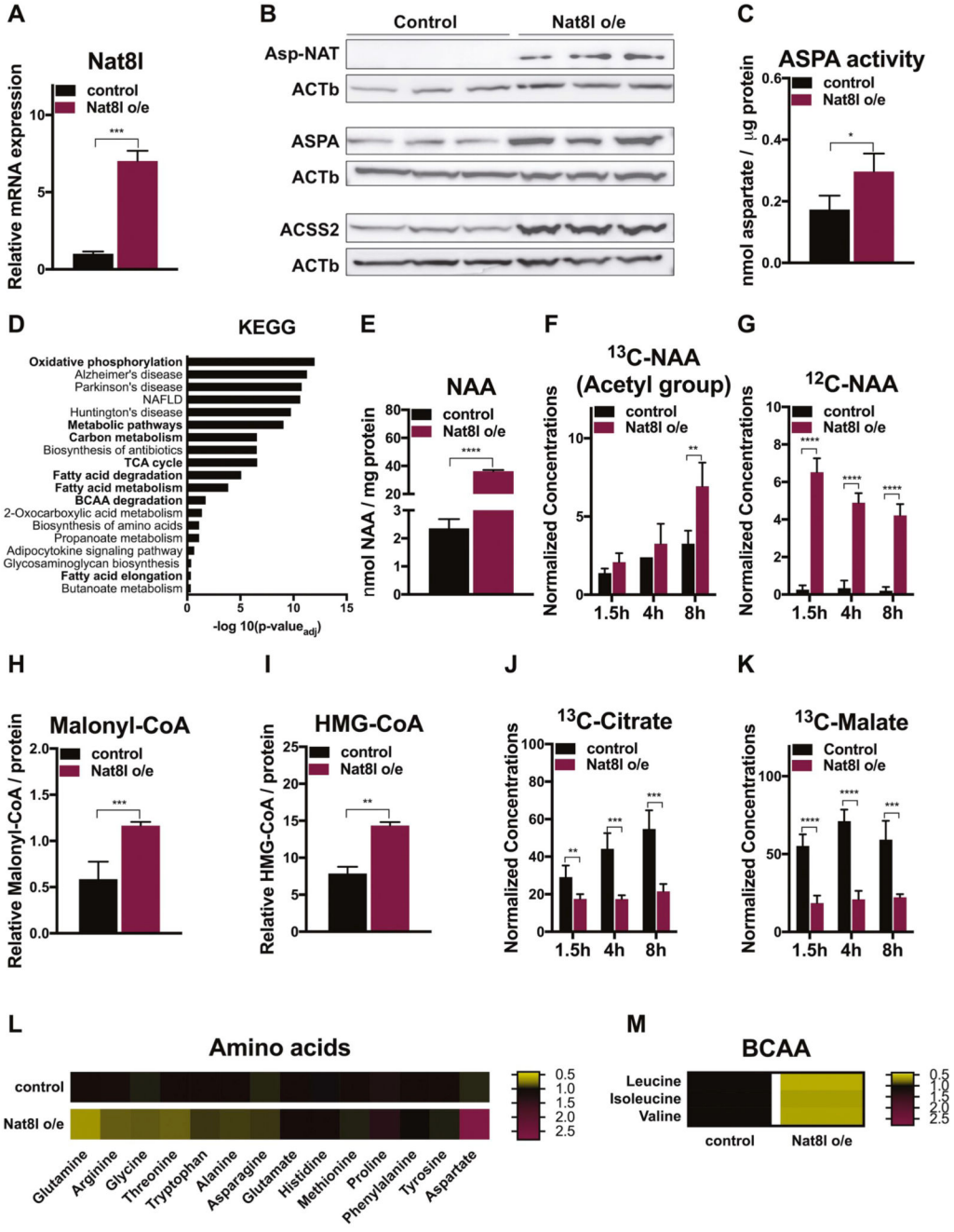

Fig. 2. The NAA pathway affects metabolic pathways, lipid synthesis and energy metabolism.

Mature iBACs with stable overexpression of Nat8l (Nat8l o/e) or control cells were used for the analysis. (A) Analysis of *Nat8l* mRNA expression. (B) Analysis of Asp-NAT, ASPA and ACSS2 protein expression ($n = 3$). (C) Aspa activity was determined by fluorometric detection of aspartate ($n = 3$). (D) Transcriptomics of 250 genes up-regulated by Nat8l o/e were submitted to DAVID functional annotation using KEGG pathways. Count shows the number of mapped genes. Benjamini-Hochberg's correction was used for adjusting *p*-value for multiple testing. (E) NAA concentration in iBACs analyzed with HPLC/HRMS ($n = 3$).

Europe PMC Funders Author Manuscripts

(F–G) ^{13}C-labeled metabolite concentrations measured by NMR after cultivating iBACs for indicated time points in the presence of 10 mM ^{13}C-glucose. Metabolite concentration was normalized to internal scaling factor ($n = 5$). (H–I) Metabolites measured by HPLC/HRMS ($n = 3$). (J–K) ^{13}C metabolite concentrations measured by NMR after cultivating iBACs for indicated time points in the presence of 10 mM ^{13}C-glucose. Metabolite concentration was normalized to internal scaling factor ($n = 5$). (L) Fold change of measured amino acids by HPLC/HRMS. Significantly reduced and increased amino acids are depicted in yellow and red, respectively ($n = 3$). (M) Fold change of BCAA measured by NMR ($n = 3$). If not otherwise mentioned, data are shown as mean ± SD. Statistical significance was calculated using two-tailed Student's *t*-test (*$p < 0.05$, **$p < 0.01$, ***$p < 0.001$, ****$p < 0.0001$). (For interpretation of the references to color in this figure legend, the reader is referred to the web version of this article.)

Europe PMC Funders Author Manuscripts

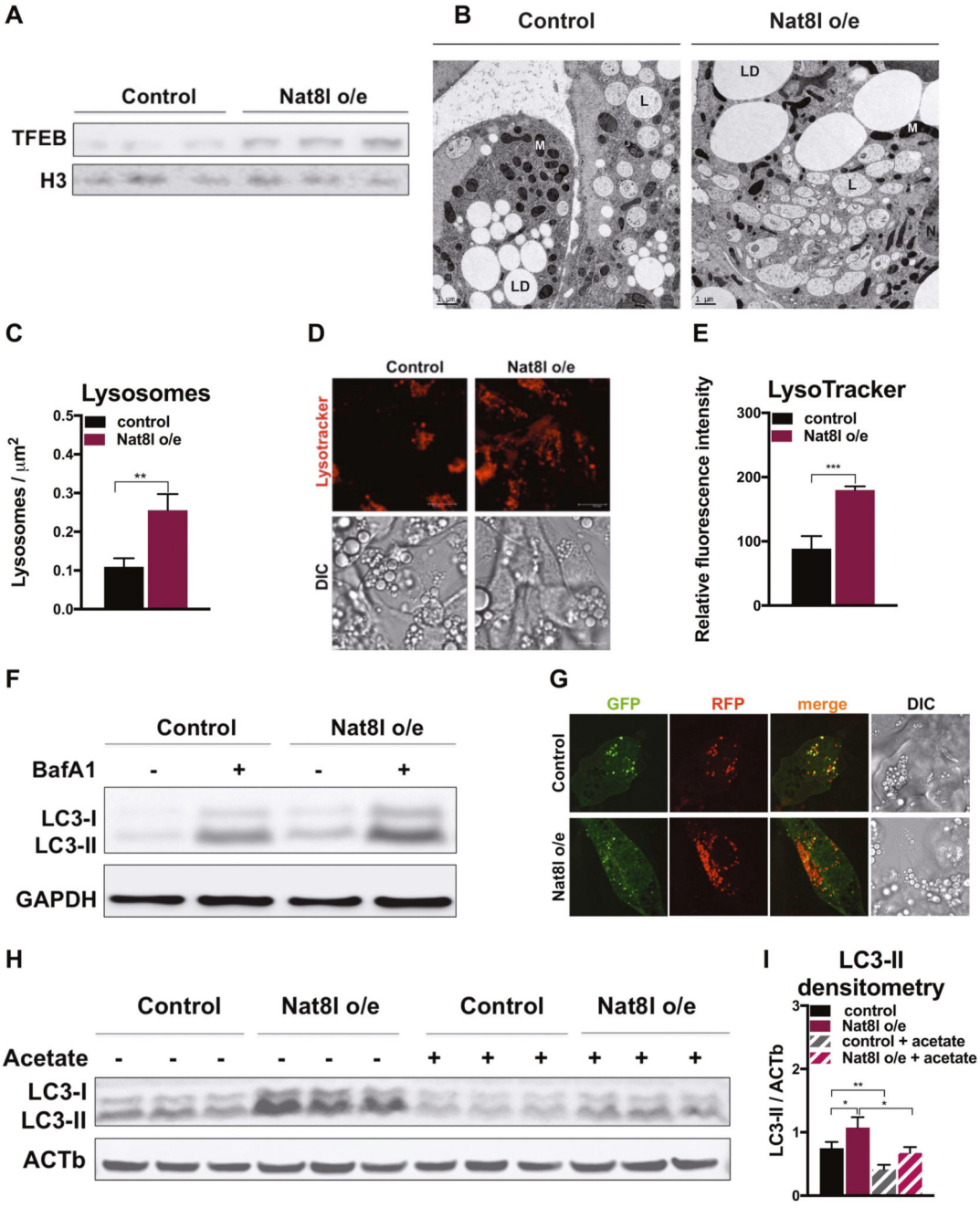

Fig. 3. Increased NAA pathway activity elevated the number of lysosomes and induced autophagy.

Mature control and Nat8l o/e iBACs were used for the analysis. (A) Immunoblot of nuclear fraction showing transcription factor EB (TFEB) translocation to the nuclei. Histone H3 was used as loading control for nucleus fraction ($n = 3$). (B) Representative electron micrographs of control and Nat8l o/e iBACs and (C) corresponding number of lysosomes, counted from all 90 electron micrographs from 3 biological replicates. Scale bar = 1 μm. L: lysosome, LD: lipid droplet, M: mitochondria N: nucleus. (D) Representative confocal image of iBACs stained with LysoTracker Red ($n = 3$). (E) Number of Lysotracker Red stained lysosomes

counted by flow cytometry ($n = 3$). (F) Autophagic flux was monitored by immunoblotting against LC3 in the presence or absence of autophagy inhibitor bafilomycin A1 (BafA1) GAPDH was used as loading control ($n = 3$). (G) Representative confocal images of cells transfected with tandem mRFP-GFP-LC3 vector. GFP and mRFP channels are shown in green and red, respectively. Elevated number of autolysosomes (red puncta in merged image) indicates increased autophagic flux. (H) Immunoblot showing LC3 in cell lysates with or without acetate supplementation to growth media (48 h, 10 mM NaAc) ($n = 3$). (I) Densitometry of LC3-II bands from (I) normalized to ACTb ($n = 3$). Data are shown as mean ± SD. Statistical significance was calculated using two-tailed Student's *t*-test (*$p < 0.05$, **$p < 0.01$, ***$p < 0.001$). (For interpretation of the references to color in this figure legend, the reader is referred to the web version of this article.)

Europe PMC Funders Author Manuscripts

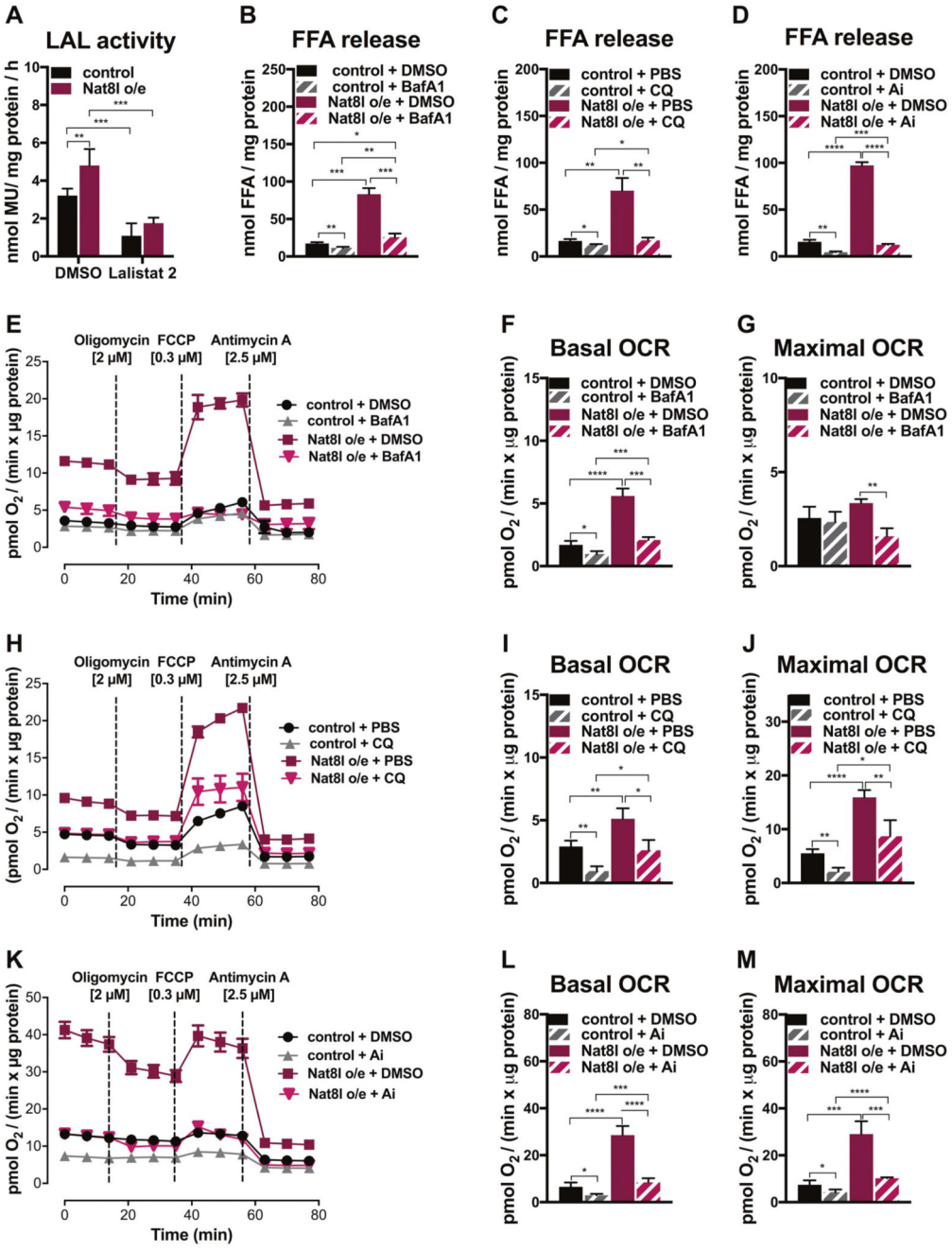

Fig. 4. Increased lipid catabolism and cellular respiration in Nat8l o/e cells is mediated by acid and neutral lipolysis.

Mature control and Nat8l o/e iBACs were used for the analysis. (A) Lysosomal acid lipase (LAL) activity in presence or absence of LAL inhibitor Lalistat 2 measured by fluorometric assay ($n = 3$). (B) Free fatty acid (FA) release into culture medium with and without 10 nM BafA1 treatment for 48 h ($n = 3$). (C) Free FA release into culture medium with and without 40 µM chloroquine (CQ) treatment for 48 h ($n = 3$). (D) Free FA release into culture medium with and without addition of 40 µM atglistatin (Ai) for 48 h ($n = 4$). (E) Oxygen consumption rate (OCR) measured with the Seahorse extracellular flux analyzer® in

presence or absence of 100 nM BafA1 2 h prior to and during the measurement. Cells were treated at the indicated time points with 1 μM oligomycin, 2 μM carbonyl cyanide *p*-trifluoromethoxyphenylhydrazone, and 2.5 μM antimycin A ($n = 4$). (F) Basal OCR was derived by subtracting non-mitochondrial respiration ($n = 4$). (G) Maximal OCR of iBACs after stimulation with 0.3 μM FCCP ($n = 4$). (H) OCR (I) basal respiration (J) maximal respiration of cells treated with 40 μM CQ for 2 h prior to and during the measurement ($n = 3$). (K) OCR (L) basal respiration and (M) maximum OCR in iBACs treated with 40 μM Ai for 2 h prior to and during the measurement ($n = 4$). Data are shown as mean ± SD. (E, H, K) Data are shown as mean ± SEM. Statistical significance was calculated using two-tailed Student's *t*-test (*$p < 0.05$, **$p < 0.01$, ***$p < 0.001$, ****$p < 0.0001$).

Europe PMC Funders Author Manuscripts

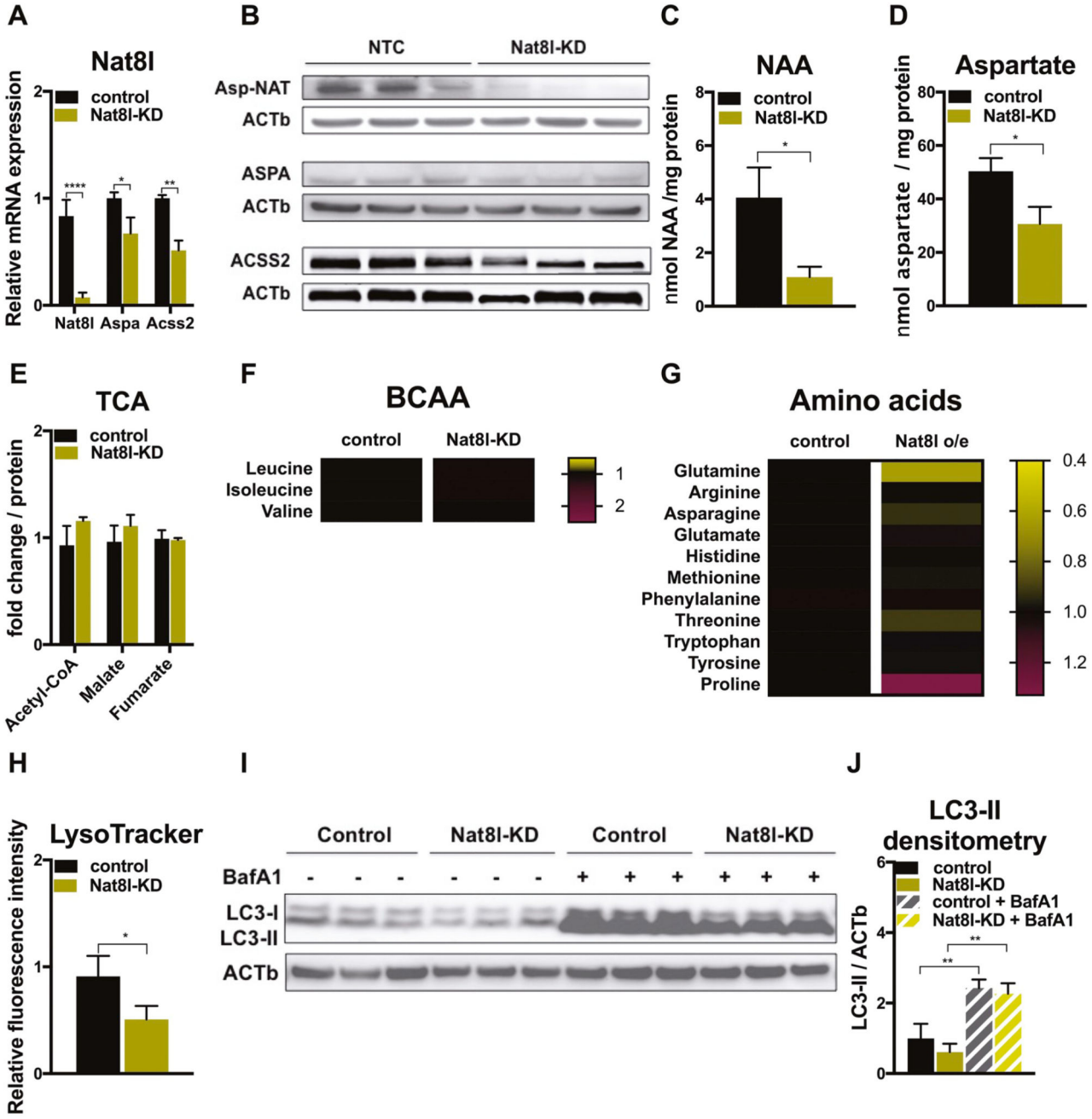

Fig. 5. Impact of Nat8l knockdown on energy metabolism, lysosomal biogenesis and autophagy.

Mature iBACs with stable knock-down of Nat8l (Nat8l-KD) or control cells were used for the analysis. (A) Analysis of *Nat8l*, *Aspa*, and *Acss2* mRNA expression ($n = 3$). (B) Asp-NAT, ASPA and ACSS2 protein expression ($n = 3$). (C–D) NAA and aspartate concentration in iBACs analyzed with HPLC/HRMS ($n = 3$). (E) TCA cycle metabolites measured by HPLC/HRMS ($n = 3$). (F) Fold change of BCAA measured by NMR ($n = 3$). (G) Fold change of amino acids measured by HPLC/HRMS. Significantly reduced and increased AA are depicted in yellow and red, respectively ($n = 3$). (H) Number of Lysotracker Red stained

lysosomes counted by flow cytometry ($n = 3$). (I) Autophagic flux was monitored by immunoblotting against LC3 in presence or absence of inhibitor bafilomycin A1 (BafA1) ($n = 3$). (J) Densitometry of LC3-II bands from (I) normalized to ACTb ($n = 3$). Data are shown as mean ± SD. Statistical significance was calculated using two-tailed Student's *t*-test (*$p < 0.05$, **$p < 0.01$, ****$p < 0.0001$). (For interpretation of the references to color in this figure legend, the reader is referred to the web version of this article.)

Europe PMC Funders Author Manuscripts